

CF₄ Capture and Separation of CF₄–SF₆ and CF₄–N₂ Fluid Mixtures Using Selected Carbon Nanoporous Materials and Metal–Organic Frameworks: A Computational Study

Ioannis Skarmoutsos,* Emmanuel N. Koukaras,* and Emmanuel Klontzas*



Cite This: *ACS Omega* 2022, 7, 6691–6699



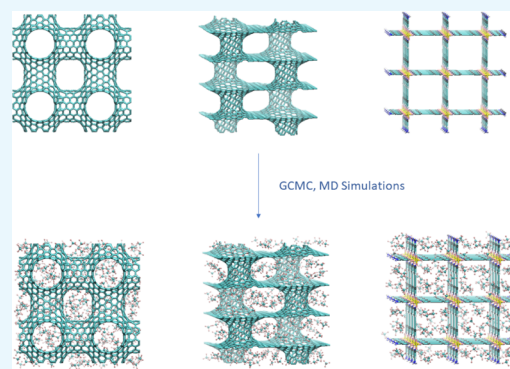
Read Online

ACCESS |

Metrics & More

Article Recommendations

ABSTRACT: The adsorption of pure fluid carbon tetrafluoride and the separation of CF₄–SF₆ and CF₄–N₂ fluid mixtures using representative nanoporous materials have been investigated by employing Monte Carlo and molecular dynamics simulation techniques. The selected materials under study were the three-dimensional carbon nanotube networks, pillared graphene using carbon nanotube pillars, and the SIFSIX-2-Cu metal–organic framework. The selection of these materials was based on their previously reported efficiency to separate fluid SF₆–N₂ mixtures. The pressure dependence of the thermodynamic and kinetic separation selectivity for the CF₄–SF₆ and CF₄–N₂ fluid mixtures has therefore been investigated, to provide deeper insights into the molecular scale phenomena taking place in the investigated nanoporous materials. The results obtained have revealed that under near-ambient pressure conditions, the carbon-based nanoporous materials exhibit a higher gravimetric fluid uptake and thermodynamic separation selectivity. The SIFSIX-2-Cu material exhibits a slightly higher kinetic selectivity at ambient and high pressures.



1. INTRODUCTION

One of the main aims of international environmental treaties and agreements, such as the Kyoto Protocol and the Paris Agreement within the United Nations Framework Convention on Climate Change, is to reduce greenhouse gas emissions in the atmosphere in order to prevent dangerous anthropogenic interference with the climate system.^{1,2} For this reason, six categories of greenhouse gases, sometimes also distinguished as CO₂³ and non-CO₂ ones,⁴ have been classified among the most potent ones. These greenhouse gases are carbon dioxide (CO₂), methane (CH₄), nitrous oxide (N₂O), hydrofluorocarbons, perfluorocarbons (PFCs), and sulfur hexafluoride (SF₆).

Among the non-CO₂ greenhouse gases, tetrafluoromethane (CF₄), the simplest PFC, has a very long atmospheric lifetime (50,000 years) and a 100 year global warming potential of 6630–7390.⁵ Although its concentration in the atmosphere is low (around 74 ppt), CF₄ contributes significantly to the greenhouse effect.⁶ Therefore, its capture or recovery from CF₄/N₂ mixtures from industrial emission sources,^{7,8} mainly associated with the aluminum production and semiconductor fabrication processes, is considered important for the reduction of global warming. Moreover, the recycle of CF₄ from CF₄/N₂ mixtures is also important in a wide range of applications involving a positron trap⁹ since these mixtures are used as buffer gases for the cooling of positrons.¹⁰

The recovery and recycle of CF₄ are also highly important in mixtures with SF₆ having significant technological applications. Mixtures of CF₄ with SF₆ are used as insulating and arc-quenching media^{11–18} at very low temperatures, down to –50 °C, especially in circuit breakers operating at these low temperatures.¹¹ In these mixtures, CF₄ is added in order to avoid liquefaction of SF₆ gas at low temperatures. These mixed gas circuit breakers are installed in converting stations, where alternating current is converted to direct current. The direct current is subsequently transmitted over long distances on a high-voltage direct current transmission line. According to the recent climate negotiation in Paris, a speedy implementation of these networks is a main path to introduce renewable energy and to harmonize power markets.

To achieve an efficient CF₄ capture, several technologies based on thermal decomposition, plasma treatment, absorption, adsorption, cryogenic recovery, and membrane separation have been developed. Among them, physical adsorption using efficient nanoporous adsorbents^{6,7,19–33} is considered as the

Received: November 3, 2021

Accepted: January 24, 2022

Published: February 16, 2022



most competitive technology for capturing CF_4 due to its low energy consumption, low cost, and easy management. However, only some limited studies in the literature are devoted to CF_4 capture using nanoporous adsorbents. In this respect, we decided to further explore the CF_4 capture and the separation of SF_6 - CF_4 and CF_4 - N_2 fluid mixtures using some selected carbon-based nanoporous materials and metal-organic frameworks (MOFs), which have been found in our previous studies^{34–36} to be very efficient for SF_6 capture and SF_6 - N_2 fluid mixture separation. These previous studies^{34,36} had revealed that three-dimensional interconnected single-wall carbon nanotube networks and pillared graphene nanostructures, consisting of parallel graphene layers stabilized by carbon nanotubes placed vertically to the graphene planes, exhibit a significant SF_6 uptake and high adsorption selectivity for SF_6 over N_2 , in comparison with the best performing materials in the literature. Our studies³⁵ also revealed that the SIFSIX-2-Cu MOF exhibits high thermodynamic and kinetic adsorption selectivity for SF_6 over N_2 .

Based on these findings, the aim of the present study was to further explore the efficiency of these different types of nanoporous materials in capturing CF_4 and separating SF_6 - CF_4 and CF_4 - N_2 fluid mixtures, using a combination of force field-based grand canonical Monte Carlo (GCMC) and molecular dynamics (MD) simulations. This paper is organized as follows: the employed computational methodology is presented in Section 2, the results and corresponding discussion in Section 3, and finally, the concluding remarks are summarized in Section 4.

2. COMPUTATIONAL METHODS

As mentioned in the introduction, two types of carbon-based nanoporous materials were investigated in the framework of the present study. The first type is a porous nanotube network (PNN),³⁷ composed of (8,8) single-walled carbon nanotubes which are connected through junctions, forming a three-dimensional cubic carbon nanotube network with an intertube distance of 11 Å and a corresponding three-dimensional porous network. The second type is the PILS pillared graphene that^{34,38} consisted of parallel graphene layers stabilized by carbon nanotubes placed vertically to the graphene planes. The pillared graphene nanostructure investigated in the present study is composed of (6,6) single-walled carbon nanotubes, with a nanotube diameter of 8.142 Å, which act as pillars between adjacent graphene layers. In this specific nanostructure, the interlayer distance is 11.2 Å and the intertube one is 20.9 Å. The supercells used in our simulations comprised $1 \times 1 \times 1$ unit cells in the case of PNN and $1 \times 1 \times 2$ unit cells in the case of PILS. The PNN supercell is cubic with a 41 Å dimension, whereas the PILS supercell is orthorhombic, with dimensions 42.60 Å \times 39.35 Å \times 44.84 Å.

The third nanoporous material taken into account in the present investigation is the $[\text{Cu}(4,4'\text{-dipyridylacetylene})_2(\text{SiF}_6)]_n$ MOF, named SIFSIX-2-Cu, resembling pillared square grids with a pore dimension of 13.05 Å. This particular MOF was synthesized by pillaring two-dimensional nets of organic ligands and metal nodes with hexafluorosilicate (SiF_6^{2-}) anions to form three-dimensional networks with primitive cubic topology.³⁹ The SIFSIX-2-Cu supercell was constituted by a $3 \times 3 \times 5$ replica of its unit cell, which was geometry optimized in our previous studies at the periodic density-functional theory level.³⁵ As mentioned in our previous studies, the SIFSIX-2-Cu supercell was saturated by adding terminal $-\text{NH}_2$ groups, and

the charges of the terminal atoms were adjusted in order to give a total zero charge to the supercell.³⁵ The supercell dimensions are 41.25 Å \times 41.25 Å \times 42.01 Å. Further details about the special characteristics of all the investigated nanomaterials can be found in our previous studies.^{34–36}

A combination of force field-based GCMC and MD simulations was employed to explore the adsorption of pure fluid CF_4 in PNN, PILS, and SIFSIX-2-Cu and the separation of the CF_4/SF_6 (two bulk molar compositions CF_4/SF_6 : 1:1 and 9:1) and CF_4/N_2 binary mixtures (bulk molar composition CF_4/N_2 : 1:9). These simulations were performed at 303 K and in the pressure range 0.1–20 bar. The well-established all-atom rigid potential model for SF_6 developed by Dellis and Samios⁴⁰ and the TraPPE potential model for N_2 ⁴¹ have been selected to be employed in our simulation studies. According to the literature,^{40,41} these models provide very accurate description of fluid properties of SF_6 and N_2 under a wide range of thermodynamic conditions and the vapor-liquid coexistence curve and critical points of the pure systems. The intramolecular geometries, charges, and Lennard-Jones 12–6 potential parameters of all the interaction sites in the potential model of SF_6 can also be found in a previous study of one of the authors in the literature,³⁵ whereas the corresponding ones for N_2 can be found in the previous study of Potoff and Siepmann.⁴¹ The OPLS rigid potential model⁴² has been employed for CF_4 . The intramolecular geometries, charges, and Lennard-Jones 12–6 potential parameters of all the interaction sites in the employed potential models of CF_4 , SF_6 , and N_2 are presented in Table 1.

Table 1. Partial Charges and Lennard-Jones 12–6 Parameters Corresponding to Each Type of Interaction Site in the Employed Potential Models of CF_4 , SF_6 , and N_2 ^a

| interaction site | q (el) | σ (Å) | ϵ (K) |
|------------------|----------|---------------|----------------|
| | | CF_4 | |
| C | 0.48 | 3.50 | 48.8126 |
| F | −0.12 | 2.95 | 26.6708 |
| | | SF_6 | |
| S | 0.66 | 3.228 | 165.14 |
| F | −0.11 | 2.947 | 27.02 |
| | | N_2 | |
| N | −0.482 | 3.31 | 36.0 |
| COM | 0.964 | | |

^aC–F bond length: 1.332 Å, S–F bond length: 1.564 Å, and N–N bond length: 1.1 Å.

The carbon atoms in the PNN and PILS materials are not charged and interact via a Lennard-Jones 12–6 potential having $\epsilon_{\text{CC}} = 28.2$ K and $\sigma_{\text{CC}} = 3.4$ Å. The partial charges and Lennard-Jones parameters corresponding to each type of atom in the SIFSIX-2-Cu material are also presented in our previous studies.³⁵

The reproducibility of the vapor-liquid equilibrium (VLE) curve is of foremost importance during adsorption studies. Thus, in order to further validate the selected force field for CF_4 and SF_6 , the VLE T - ρ curves have been calculated using NVT Gibbs ensemble Monte Carlo (GEMC) simulations⁴³ and compared to available experimental data.

The RASPA Monte Carlo simulation code⁴⁴ was used in order to perform the GCMC and GEMC simulations. The fugacities of the adsorbed species, which were used as inputs for the GCMC simulations, were calculated by employing the Peng–Robinson equation of state.⁴⁵ For each simulated thermody-

dynamic condition, 10^5 Monte Carlo cycles were performed for the equilibration and production runs. In these Monte Carlo cycles, different types of trial moves were attempted, including creation or deletion of molecules, translation or rotation, and exchange of the molecular identity. Note that the calculated error bars in the calculated fluid uptakes in the case of the GCMC simulations were in the range of about 1%. The corresponding error bars in the calculated gas and liquid densities in the cases of the GEMC simulations were in the range 0.4–2.0%, with the largest values observed under thermodynamic conditions approaching the critical point. NVT-MD simulations were subsequently carried out to calculate the self-diffusion coefficients of the components of the investigated adsorbed mixtures at the ambient pressure of 1 bar and the high pressure of 20 bar. The MD simulations were performed for all the adsorbed mixtures corresponding to each one of the investigated nanoporous materials. The integration of the equations of motion was achieved by employing the well-established leapfrog-type Verlet algorithm⁴⁶ and using an integration time step of 1 fs. The intramolecular geometry of SF₆, CF₄, and N₂ molecules was constrained using the quaternion formalism.⁴⁶ A Nose–Hoover thermostat with a temperature relaxation time of 0.5 ps was used to constrain the temperature during the simulations.⁴⁷ A 12 Å cutoff was used to treat the short-range interactions, and long-range corrections for the Lennard-Jones interactions were also taken into account in all MD and MC simulations. Test simulation runs, employing higher cutoffs (15 and 18 Å), have shown that when using the long-range corrections for the Lennard-Jones interactions, the results obtained converge for all the investigated cutoffs. The long-range electrostatic interactions were also treated using the standard Ewald summation method.⁴⁶ All MD simulations were run for 5 ns, after a 1 ns equilibration period, using the DL_POLY simulation code.⁴⁸ During the simulations, the intramolecular geometries of the adsorbents were kept rigid.

3. RESULTS AND DISCUSSION

3.1. VLE of CF₄ and SF₆. The NVT-GEMC simulations for the calculation of the VLE T – ρ curves were performed at eight experimentally available coexistence points in the temperature range 130–200 K for pure CF₄ and in the range 230–300 K for pure SF₆. The simulated systems consisted of 320 CF₄ and SF₆ molecules, equally distributed to the two simulated systems. The molecules in the initial configurations in each subsystem were randomly placed. The density of the two subsystems was set to $(\rho_l + \rho_v)/2$, where ρ_l and ρ_v are the experimental values of the density of the liquid and vapor phase at each investigated temperature, respectively. The calculated T – ρ vapor–liquid coexistence curves for pure CF₄ and SF₆ are presented in Figure 1, along with the experimental ones.

Apparently, the good agreement between the calculated and experimental data can be clearly observed. Moreover, the critical density and temperature of CF₄ and SF₆ were estimated by using the well-known critical scaling relation and the law of rectilinear diameters⁴⁹

$$\rho_l - \rho_v = B \cdot (T_c - T)^\beta \quad (1)$$

$$\frac{\rho_l + \rho_v}{2} = \rho_c + A \cdot (T - T_c) \quad (2)$$

The estimated critical values (T_c, ρ_c) for CF₄ were $T_c = 239.3$ K and $\rho_c = 0.6078$ g/cm³, which are in reasonable agreement with the experimental ones (227.5 K, 0.6257 g/cm³) and much closer to the experiment compared to the values predicted by

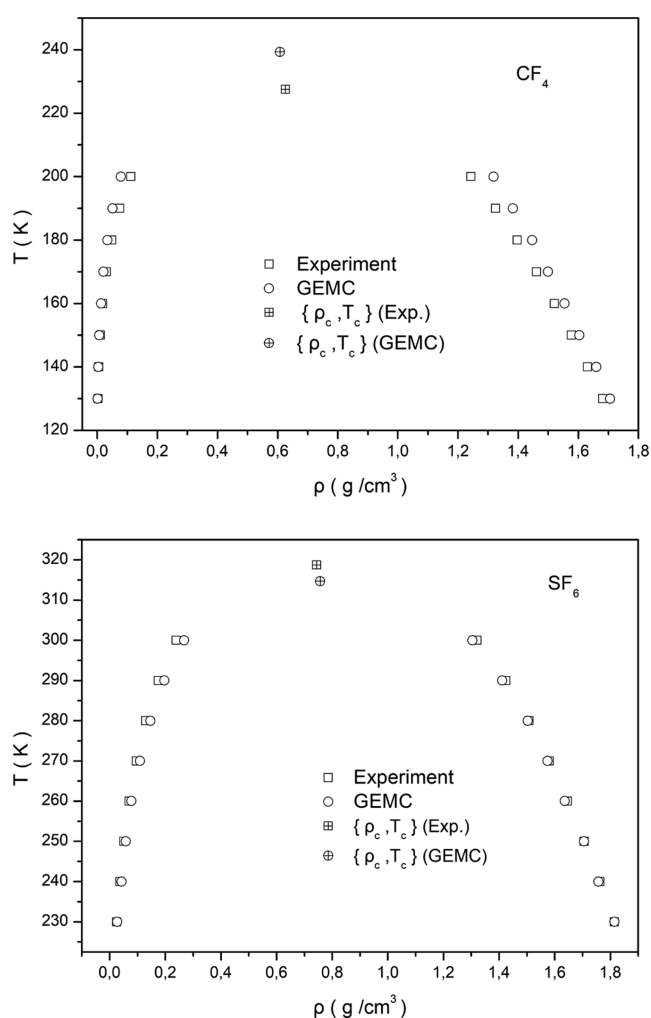


Figure 1. Calculated, from GEMC simulations, T – ρ vapor–liquid coexistence curves of pure CF₄ and SF₆, plotted together with the experimental ones. The estimated critical points are also presented in comparison with the experiments.

other force fields of CF₄, presented in previous studies in the literature.⁵⁰ Similarly, the estimated critical values (T_c, ρ_c) for SF₆ were $T_c = 314.7$ K and $\rho_c = 0.757$ g/cm³, which are also in good agreement with the experimental ones (318.7 K, 0.743 g/cm³).⁴⁰ Note also that the critical exponent β in eq 1 has been estimated to be 0.3105 and 0.3119 in the cases of CF₄ and SF₆, respectively. Consequently, the employed force fields of CF₄ and SF₆ provide realistic descriptions of the VLE, which according to the literature,⁵¹ is of paramount importance in adsorption studies.

3.2. Pure CF₄ Adsorption. The gravimetric adsorption isotherms of pure CF₄ at 303.15 K and in the pressure range 0.1–20 bar for all the investigated materials are illustrated in Figure 2. Apparently, the CF₄ gravimetric uptake is higher in the case of PNN at the low-pressure range, up to about 5 bar. However, at higher pressures, the gravimetric uptake in the case of PILS and SIFSIX-2-Cu is higher due to the larger free volume of these materials. For instance, at ambient pressure (1 bar), the calculated CF₄ uptake in the PNN, PILS, and SIFSIX-2-Cu materials is 4.89, 3.33, and 1.49 mmol/g, respectively. These values are among the highest reported regarding the uptake of CF₄ at ambient pressure, when compared to previous studies for several nanoporous materials in the literature.³² At 20 bar, the

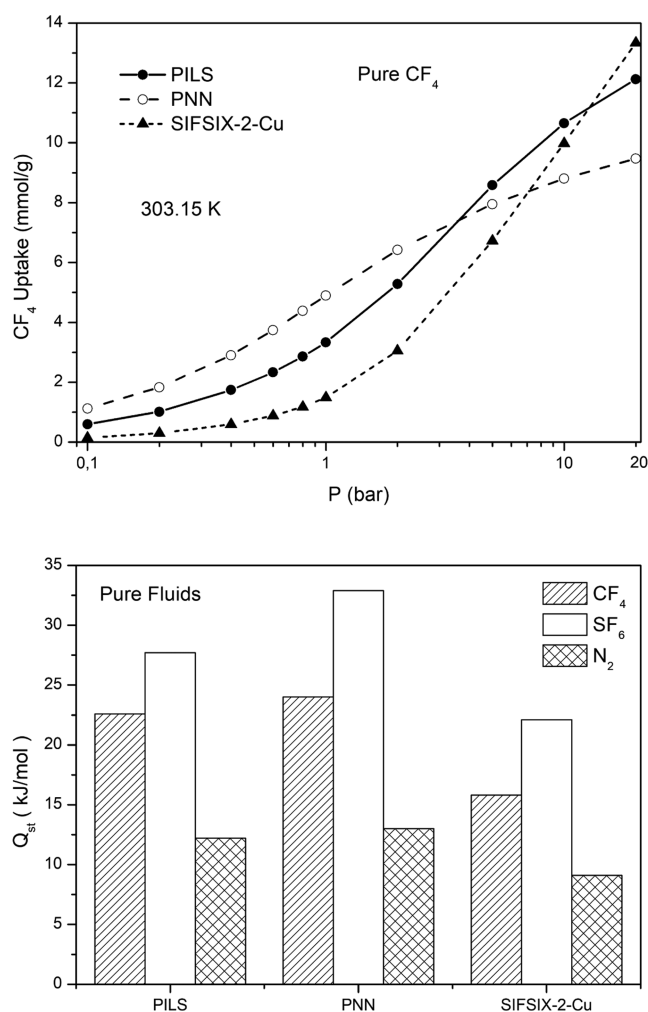


Figure 2. Gravimetric adsorption isotherms of pure CF₄ at 303.15 K up to 20 bar (top) and isosteric heat of adsorption in the low coverage for CF₄, SF₆, and N₂ (bottom).

corresponding values for PNN, PILS, and SIFSIX-2-Cu are 9.48, 12.12, and 13.34 mmol/g, respectively. Representative snapshots, depicting the adsorbed CF₄ molecules in the investigated materials at 1 and 20 bar, are presented in Figure 3. Within the pressure range studied, it can be deduced that the saturation has not been achieved for any of the adsorbents considered here. To evaluate the interaction strength between the adsorbents and the adsorbates, the isosteric heat of adsorption (Q_{st}) was calculated at low coverage, corresponding to the pressure of 0.1 bar, which is also presented in Figure 2. The calculated isosteric heat of adsorption of pure CF₄, obtained in the framework of this study, is presented together with the calculated values for pure SF₆ and N₂, which were obtained in our previous studies.^{35,36} Regarding pure CF₄ adsorption, the highest predicted isosteric heat of adsorption at low coverage is observed in the case of PNN (24.0 kJ/mol), followed by PILS (22.6 kJ/mol), whereas the lowest value of Q_{st} corresponds to SIFSIX-2-Cu (15.8 kJ/mol). The higher uptake of CF₄ at low pressures in the case of PNN can be explained in terms of the calculated Q_{st} of pure CF₄ at low coverage. The trends observed for the values of Q_{st} corresponding to each one of the investigated materials are consistent with the corresponding trends regarding the CF₄ adsorption at low pressures, further confirming that the CF₄ adsorption at low pressures is thermodynamically driven. The

same trends have also been observed in the case of the pure SF₆ and N₂ adsorption. Nevertheless, in the case of SF₆, the calculated Q_{st} values are higher in comparison with CF₄. The corresponding Q_{st} values for PNN, PILS, and SIFSIX-2-Cu in the case of pure SF₆ adsorption are 32.9, 27.7, and 22.1 kJ/mol, respectively. In the case of pure N₂ adsorption, the corresponding Q_{st} values are significantly lower. The calculated Q_{st} values for PNN, PILS, and SIFSIX-2-Cu in the latter case are 13.0, 12.2, and 9.1 kJ/mol, respectively.

3.3. Separation of CF₄/SF₆ Fluid Mixtures. Subsequently, as mentioned in Section 2, GCMC simulations were performed in order to calculate the co-adsorption isotherms of CF₄/SF₆ fluid mixtures. Two bulk molar compositions (CF₄/SF₆: 1:1 and 9:1) were taken into account in our calculations, and the results obtained for the PNN, PILS, and SIFSIX-2-Cu materials are presented in Figure 4.

Apparently, the molar fraction of the binary mixture influences the co-adsorption behavior of the adsorbents. In the case of the equimolar mixture, the SF₆ co-adsorption is much more favored at low pressures, especially in the cases of PNN and PILS. This finding is consistent with the fact that the isosteric heat of adsorption of pure SF₆ at low coverage is higher in comparison with CF₄. As the pressure increases, we observe an increase in the loading of CF₄ that keeps the loading of SF₆ almost constant for PNN and PILS. In contrast, the sulfur hexachloride loading of SIFSIX-2-Cu exhibits a continuous increase and surpasses the corresponding loading of the carbon-based adsorbents. This reveals that the thermodynamically driven favored adsorption of SF₆ becomes less pronounced in higher pressures, as attributed to two reasons. The first one is related to the larger size and kinetic diameter of SF₆ with respect to CF₄. Additionally, size- and shape-dependent packing effects start to play an important role. The same reasons have a dominant role in the case of the binary mixture containing 10% sulfur hexafluoride. For this mixture composition, increased loading for SF₆ is observed in the pressure range below 2 bar, which is more pronounced for PNN and PILS. At higher pressures, there is a clear enhancement of the CF₄ loading, exceeding the loading of SF₆ for the adsorbents under study. This is an indication of the high competitiveness of both molecules to occupy the available free volume, leading to the displacement of SF₆ at high pressures. Thus, the selectivity will be reduced at high pressures.

The trends observed in the calculated co-adsorption isotherms coupled with the values obtained for Q_{st} are more clearly reflected on the calculated values of the thermodynamic adsorption selectivity $S_{(SF_6/CF_4)}$

$$S_{(SF_6/CF_4)} = \left(\frac{x_{SF_6}}{x_{CF_4}} \right) \left(\frac{y_{CF_4}}{y_{SF_6}} \right) \quad (3)$$

where x_i and y_i are the molar fractions of each component i ($i = SF_6, CF_4$) in the adsorbed and bulk phases, respectively. The calculated thermodynamic adsorption selectivity $S_{(SF_6/CF_4)}$ for the investigated fluid mixture as a function of pressure at 303.15 K is presented in Figure 5. The thermodynamic adsorption selectivity decreases with the increase in the pressure in the cases of PNN and PILS for both mole fractions of CF₄ (0.5 and 0.9). The selectivity values observed in both cases are quite similar, with the ones corresponding to PNN being slightly higher. Interestingly, in the case of SIFSIX-2-Cu, the selectivity reaches a maximum value, which is observed at 2 and 5 bar in the cases

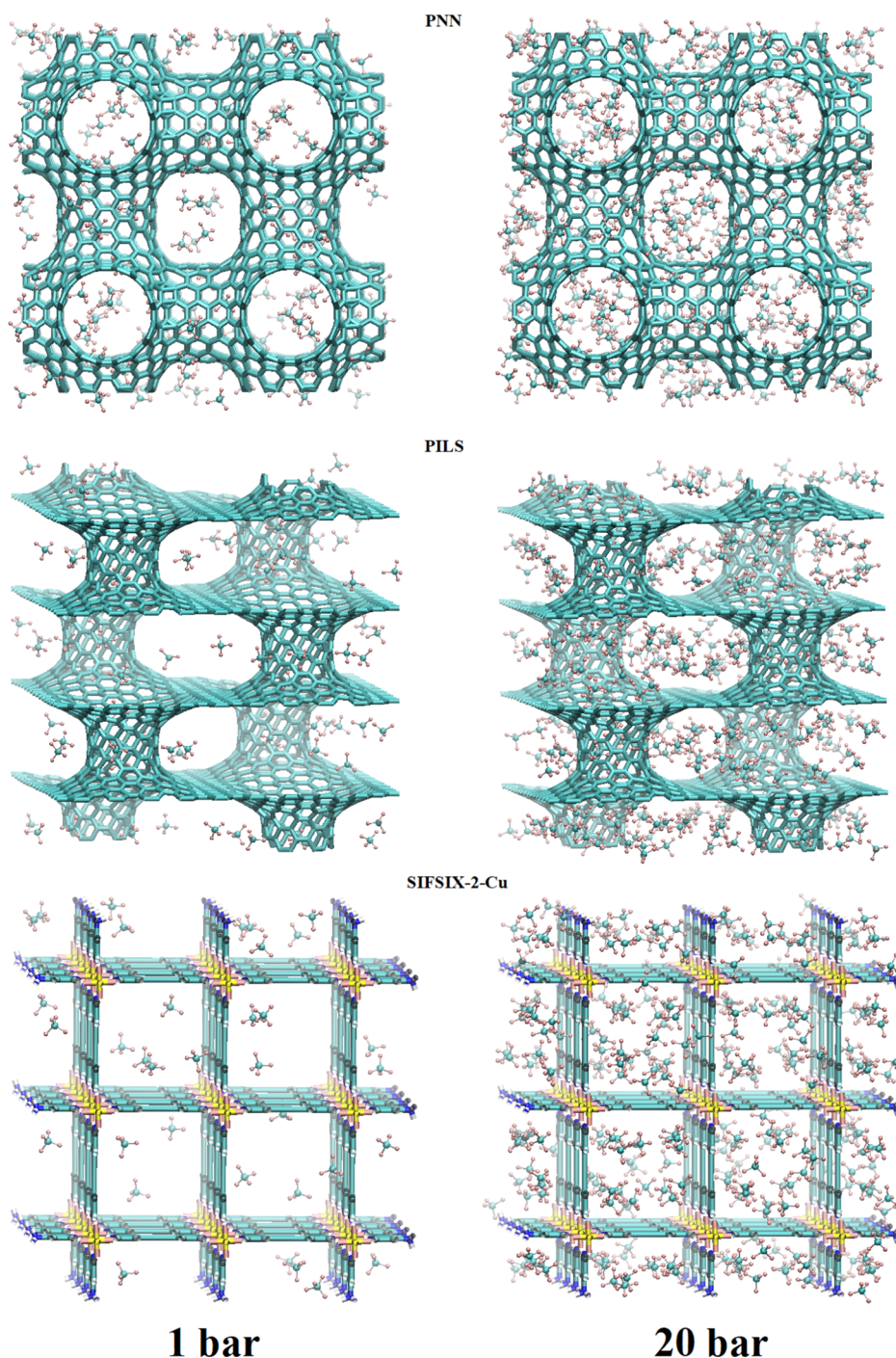


Figure 3. Representative snapshots, depicting the adsorbed CF_4 molecules in the investigated PNN, PILS, and SIFSIX-2-Cu materials at 303.15 K and $P = 1, 20$ bar.

where the bulk mole fraction of CF_4 is 0.5 and 0.9, respectively. A similar pressure dependence of the selectivity for the SF_6/N_2 separation was also observed for the SIFSIX-2-Cu nanoporous material³⁵ and the FAU-ZTC zeolite,⁵² which has a similar pore diameter with SIFSIX-2-Cu. The appearance of such a maximum, which has been observed for both the investigated bulk mixture compositions, can be interpreted in terms of competitive adsorption phenomena at high pressures. At these pressures, the adsorption of CF_4 in the nanopores is facilitated due to its smaller kinetic diameter in comparison with SF_6 . On the other hand, at lower pressures, the separation mechanism is mainly a thermodynamically driven one.^{35,52} The shift of the

selectivity maximum at higher pressures observed for the CF_4/SF_6 mixture with a 9:1 bulk molar composition can also be attributed to the lower bulk composition of SF_6 . This lower bulk composition of SF_6 leads to a more pronounced increase in the slope of the uptake of CF_4 with pressure at higher pressures in comparison with SF_6 , as it can also be observed in Figure 4, resulting in a lower $S_{(\text{SF}_6/\text{CF}_4)}$ selectivity due to packing effects.

MD simulations were further performed in the canonical NVT ensemble, using the calculated SF_6 and CF_4 uptakes corresponding to 1 and 20 bar, respectively, and the bulk mixture composition with $X_{\text{CF}_4}^{\text{bulk}} = 0.9$, to explore the diffusivity

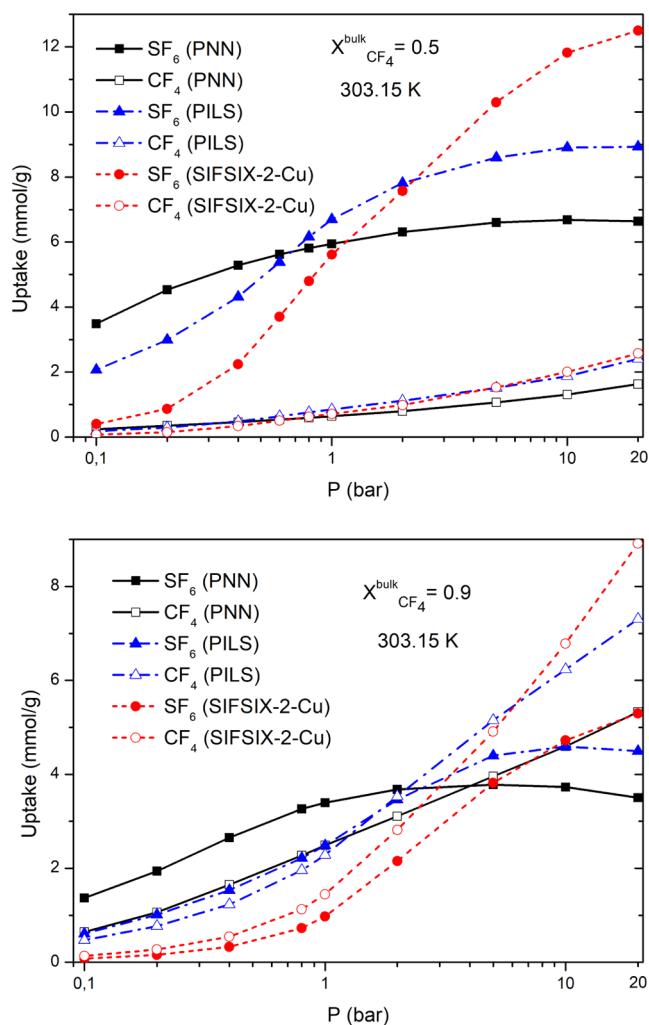


Figure 4. Calculated co-adsorption isotherms of CF_4/SF_6 fluid mixtures ($X_{\text{CF}_4}^{\text{bulk}} = 0.5, 0.9$).

of the guest molecules in the PNN, PILS, and SIFSIX-2-Cu materials. The self-diffusion coefficients of SF_6 and CF_4 were calculated using the well-known Einstein relation applied to the mean-square displacements for both guests averaged over all the MD trajectories and using a multi-time step origin. The calculated self-diffusion coefficients are presented in Table 2.

From this table, we can see that the relative percentage decrease in the self-diffusion of the adsorbed SF_6 and CF_4 molecules upon the increase in the pressure is more pronounced in the case of the PNN and PILS materials. However, the ratio $D(\text{CF}_4)/D(\text{SF}_6)$ is higher in the case of SIFSIX-2-Cu, signifying that the kinetic separation of the adsorbed mixture components is slightly more favored in SIFSIX-2-Cu.

3.4. Separation of CF_4/N_2 Fluid Mixtures. The co-adsorption isotherms of a CF_4/N_2 fluid mixture (with bulk molar composition CF_4/N_2 : 1:9) were also investigated in the present treatment, and the results obtained for the PNN, PILS, and SIFSIX-2-Cu materials are presented in Figure 6. From this figure, we can see that the actual gravimetric uptakes of each one of the mixture components are quite low at ambient pressures, and only at the high-pressure region, they exhibit values in the range 2–5 mmol/g.

The calculated values of the thermodynamic adsorption selectivity $S_{(\text{CF}_4/\text{N}_2)}$ are also presented in Figure 7. From these

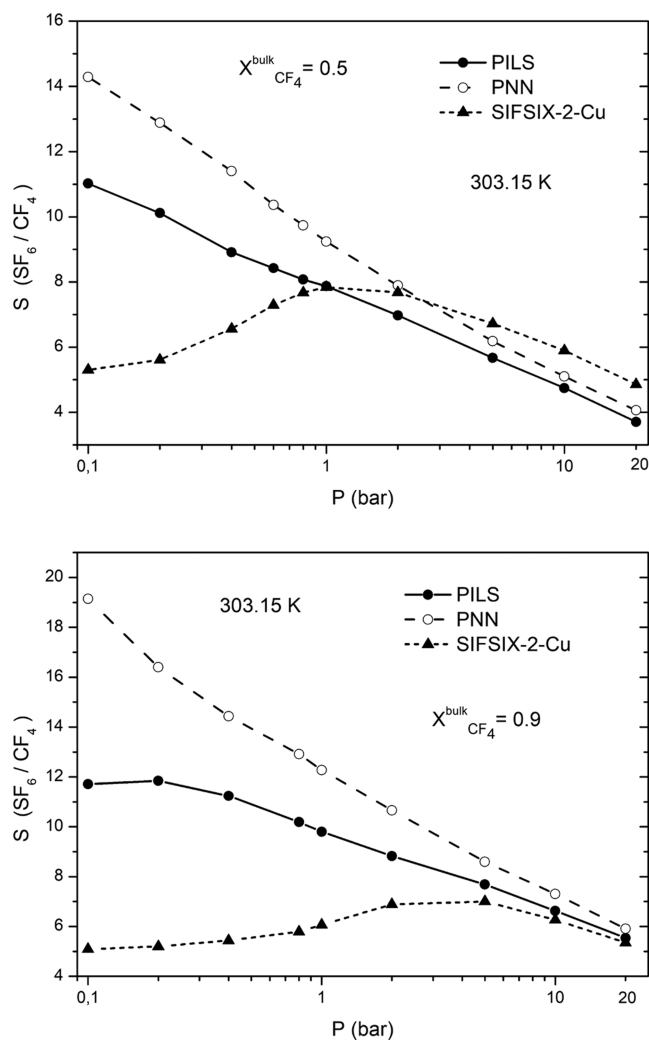


Figure 5. Pressure dependence of the calculated thermodynamic adsorption selectivity $S_{(\text{SF}_6/\text{CF}_4)}$ for the investigated fluid mixture compositions at 303.15 K.

Table 2. Calculated Self-Diffusion Coefficients of the Adsorbed SF_6 and CF_4 Molecules in the Investigated Nanomaterials, Corresponding to the Bulk Fluid Mixture with $X_{\text{CF}_4}^{\text{bulk}} = 0.9$ and Pressures of 1 and 20 bar, Respectively

| material | $D(\text{SF}_6)$ ($10^{-9} \text{ m}^2/\text{s}$) | $D(\text{CF}_4)$ ($10^{-9} \text{ m}^2/\text{s}$) | $D(\text{CF}_4)/D(\text{SF}_6)$ |
|---|--|--|---------------------------------|
| $P = 1 \text{ bar}, X_{\text{CF}_4}^{\text{bulk}} = 0.9$ | | | |
| PILS | 7.55 | 12.44 | 1.65 |
| PNN | 2.46 | 2.91 | 1.18 |
| SIFSIX-2-Cu | 2.30 | 6.81 | 2.96 |
| $P = 20 \text{ bar}, X_{\text{CF}_4}^{\text{bulk}} = 0.9$ | | | |
| PILS | 1.91 | 2.85 | 1.49 |
| PNN | 0.98 | 1.37 | 1.52 |
| SIFSIX-2-Cu | 2.12 | 3.85 | 1.82 |

figures, we can see that the thermodynamic selectivity $S_{(\text{CF}_4/\text{N}_2)}$ exhibits the highest values in the case of the carbon-based nanoporous materials, particularly for the PNN. This finding is also consistent with our previous studies,³⁴ which had revealed that the thermodynamic separation selectivity of SF_6/N_2 mixtures is significantly enhanced in the case of the PNN and

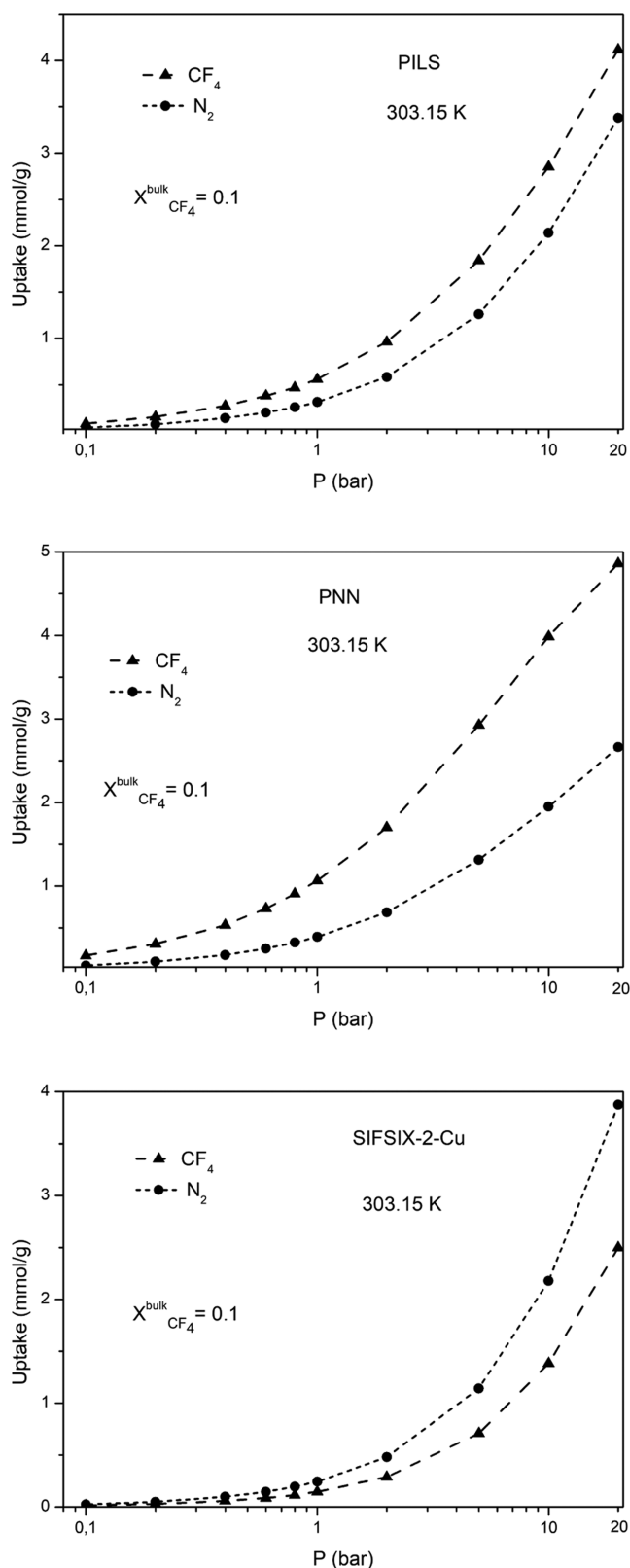


Figure 6. Calculated co-adsorption isotherms of CF_4/N_2 fluid mixtures ($X_{\text{CF}_4}^{\text{bulk}} = 0.1$).

PILS materials. However, the selectivity values observed in the case of the CF_4/N_2 mixture are significantly lower in comparison with the ones obtained for the SF_6/N_2 mixture with the same molar composition. This finding is also consistent with the lower

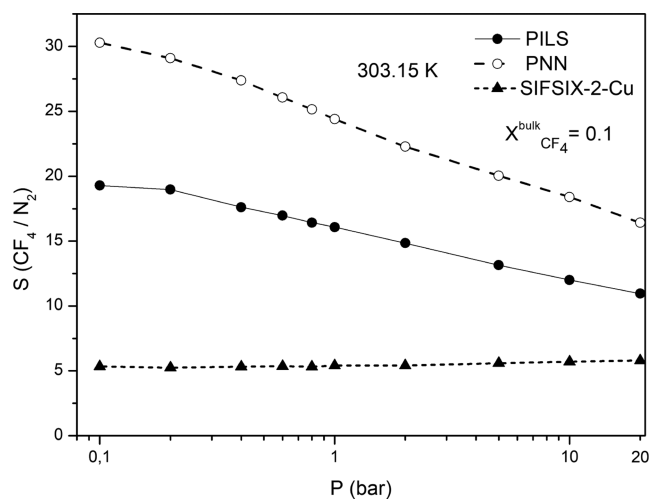


Figure 7. Pressure dependence of the calculated thermodynamic adsorption selectivity $S_{(\text{CF}_4/\text{N}_2)}$ for the investigated fluid mixture composition at 303.15 K.

isosteric heat of adsorption values Q_{st} for CF_4 in comparison with SF_6 . From Figure 7, it can also be observed that for both the PNN and PILS materials, the selectivity $S_{(\text{CF}_4/\text{N}_2)}$ values decrease with the increase in the pressure. On the other hand, in the case of SIFSIX-2-Cu, the selectivity remains almost constant along the investigated pressure range, exhibiting a value around five. The much lower selectivity value in the case of SIFSIX-2-Cu can also be attributed to the fact that the actual uptake value of CF_4 along the investigated pressure range is lower in comparison with the one corresponding to N_2 , whereas the opposite behavior is observed in the case of PNN and PILS. All these findings clearly indicate that the thermodynamic adsorption selectivity in the case of the CF_4/N_2 fluid mixture is more pronounced for the carbon-based nanoporous materials, particularly in the case of PNN.

Due to the very low uptake of the mixture components at 1 bar, MD simulations were performed in the canonical NVT ensemble using the calculated CF_4 and N_2 uptakes corresponding to 20 bar and the bulk mixture composition with $X_{\text{CF}_4}^{\text{bulk}} = 0.1$, to explore the diffusivity of the guest molecules in the PNN, PILS, and SIFSIX-2-Cu materials. The calculated self-diffusion coefficients of CF_4 and N_2 are presented in Table 3.

From this table, it can be clearly observed that the ratio $D(\text{N}_2)/D(\text{CF}_4)$ is higher in the case of SIFSIX-2-Cu, indicating that the kinetic separation of the adsorbed mixture components is more favored in SIFSIX-2-Cu, as in the case of the CF_4-SF_6 mixture.

Table 3. Calculated Self-Diffusion Coefficients of the Adsorbed N_2 and CF_4 Molecules in the Investigated Nanomaterials, Corresponding to the Bulk Fluid Mixture with $X_{\text{CF}_4}^{\text{bulk}} = 0.1$ and Pressures of 20 bar

| material | $P = 20 \text{ bar}, X_{\text{CF}_4}^{\text{bulk}} = 0.1$ | | |
|-------------|---|---|--------------------------------|
| | $D(\text{N}_2)$ ($10^{-9} \text{ m}^2/\text{s}$) | $D(\text{CF}_4)$ ($10^{-9} \text{ m}^2/\text{s}$) | $D(\text{N}_2)/D(\text{CF}_4)$ |
| PILS | 25.92 | 13.89 | 1.87 |
| PNN | 9.19 | 5.58 | 1.65 |
| SIFSIX-2-Cu | 27.65 | 7.48 | 3.70 |

4. CONCLUSIONS

The adsorption of pure fluid carbon tetrafluoride and the separation of CF_4 - SF_6 and CF_4 - N_2 fluid mixtures, using three-dimensional carbon nanotube networks (PNN), pillared graphene with carbon nanotube pillars (PILS), and the SIFSIX-2-Cu MOF, were investigated by employing a combination of Monte Carlo and MD simulation techniques. These particular nanoporous materials were selected based upon their very satisfactory performance for SF_6 capture and SF_6 - N_2 fluid mixture separation, which was revealed in our previous studies.

The results obtained regarding pure CF_4 adsorption have revealed that the highest predicted isosteric heat of adsorption at low coverage is observed in the case of PNN (24.0 kJ/mol), followed by PILS (22.6 kJ/mol), whereas the lowest value of Q_{st} corresponds to SIFSIX-2-Cu (15.8 kJ/mol). These trends are consistent with the corresponding trends regarding the gravimetric uptake of pure CF_4 adsorption at low pressures, further confirming that the CF_4 adsorption at low pressures is thermodynamically driven. However, at higher pressures, the gravimetric uptake in the case of PILS and SIFSIX-2-Cu is higher due to the larger pore dimensions of these systems.

The results obtained have also revealed that in the case of the CF_4 - SF_6 fluid mixtures, under near-ambient pressure conditions, the carbon-based nanoporous materials exhibit a higher gravimetric fluid uptake and thermodynamic separation selectivity. On the other hand, the SIFSIX-2-Cu material exhibits a higher kinetic selectivity at both ambient and high pressures. Regarding the separation of the CF_4 - N_2 mixtures, the carbon-based nanoporous materials exhibit a higher thermodynamic separation selectivity in comparison with the SIFSIX-2-Cu MOF but significantly lower in comparison with the values obtained in our previous studies for the SF_6 - N_2 mixtures. However, as for the SF_6 - CF_4 fluid mixture, the SIFSIX-2-Cu material also exhibits a higher kinetic selectivity at high pressures, in the range of 20 bar, in the case of the CF_4 - N_2 mixture.

AUTHOR INFORMATION

Corresponding Authors

Ioannis Skarmoutsos – *Theoretical and Physical Chemistry Institute, National Hellenic Research Foundation, GR-116 35 Athens, Greece; Laboratory of Quantum and Computational Chemistry, Department of Chemistry, Aristotle University of Thessaloniki, 54124 Thessaloniki, Greece;* orcid.org/0000-0002-2908-9155; Email: iskarmoutsos@hotmail.com

Emmanuel N. Koukaras – *Laboratory of Quantum and Computational Chemistry, Department of Chemistry, Aristotle University of Thessaloniki, 54124 Thessaloniki, Greece;* orcid.org/0000-0002-5069-8334; Email: koukarase@chem.auth.gr

Emmanuel Klontzas – *Theoretical and Physical Chemistry Institute, National Hellenic Research Foundation, GR-116 35 Athens, Greece;* orcid.org/0000-0002-1974-5198; Email: klontzas@eie.gr

Complete contact information is available at:
<https://pubs.acs.org/10.1021/acsomega.1c06167>

Notes

The authors declare no competing financial interest. The data that support the findings of this study are available from the corresponding author upon reasonable request.

ACKNOWLEDGMENTS

The authors acknowledge the funding from the Hellenic Foundation for Research and Innovation (HFRI) and the General Secretariat for Research and Technology (GSRT), under grant agreement no 1536.

REFERENCES

- (1) Oberthür, S.; Ott, H. E. *The Kyoto Protocol: International Climate Policy for the 21st Century*; Springer Verlag: Berlin, 1999.
- (2) Hulme, M. 1.5 °C and climate research after the Paris Agreement. *Nat. Clim. Change* **2016**, *6*, 222–224.
- (3) Lacic, A. A.; Schmidt, G. A.; Rind, D.; Ruedy, R. A. Atmospheric CO_2 : Principal Control Knob Governing Earth's Temperature. *Science* **2010**, *330*, 356–359.
- (4) Montzka, S. A.; Dlugokencky, E. J.; Butler, J. H. Non- CO_2 greenhouse gases and climate change. *Nature* **2011**, *476*, 43–50.
- (5) Vallero, D. *Air Pollution Calculations: Quantifying Pollutant Formation, Transport, Transformation, Fate and Risks*; Elsevier, 2019.
- (6) Yuan, X.; Cho, M.-K.; Lee, J. G.; Choi, S. W.; Lee, K. B. Upcycling of waste polyethylene terephthalate plastic bottles into porous carbon for CF_4 adsorption. *Environ. Pollut.* **2020**, *265*, 114868.
- (7) Choi, S. W.; Yoon, H. J.; Lee, H. J.; Lee, E.-S.; Lim, D.-S.; Lee, K. B. CF_4 adsorption on porous carbon derived from silicon carbide. *Microporous Mesoporous Mater.* **2020**, *306*, 110373.
- (8) Tsai, W.-T.; Chen, H.-P.; Hsien, W.-Y. A review of uses, environmental hazards and recovery/recycle technologies of perfluorocarbons (PFCs) emissions from the semiconductor manufacturing processes. *J. Loss Prev. Process Ind.* **2002**, *15*, 65–75.
- (9) Marjanović, S.; Banković, A.; Cassidy, D.; Cooper, B.; Deller, A.; Dujko, S.; Petrović, Z. L. A CF_4 based positron trap. *J. Phys. B: At., Mol. Opt. Phys.* **2016**, *49*, 215001.
- (10) Natisin, M. R.; Danielson, J. R.; Surko, C. M. Positron cooling by vibrational and rotational excitation of molecular gases. *J. Phys. B: At., Mol. Opt. Phys.* **2014**, *47*, 225209.
- (11) Middleton, R. L.; Eng, P. Cold-weather application of gas mixture (SF_6/N_2 , SF_6/CF_4) circuit breakers: A utility user's perspective. *1st Conference on SF6 and Environment: Emission and Reduction Strategies*, November 2000.
- (12) Liu, W.; Su, Z.; Qi, J.; Zhu, F.; Zhao, Y.; Ma, F.; Yuan, X.; Chen, Y. Application and Recycling of SF_6 gas Mixtures in Gas-insulated Circuit Breaker in Northern China. *IOP Conf. Ser.: Earth Environ. Sci.* **2017**, *69*, 012002.
- (13) Kuffel, E.; Toufani, K. Breakdown Strength of SF_6/CF_4 Mixtures in Highly Non-Uniform Fields. In *Gaseous Dielectrics VIII*; Christophorou, L. G., Olthoff, J. K., Eds.; Springer: Boston, MA, 1998.
- (14) Park, W.; Hwang, C. H.; Kim, N. R.; Lee, K. T.; Huh, C. S. Breakdown characteristics of SF_6/CF_4 mixtures in test chamber and 25.8 kV GIS. *Eng. Lett.* **2007**, *15*, 145–148.
- (15) Liu, X.; Xiao, D. Monte Carlo simulation of electron swarm parameters in the SF_6/CF_4 gas mixtures. *Jpn. J. Appl. Phys., Part 1* **2007**, *46*, 1663–1667.
- (16) de Urquijo, J.; Basurto, E.; Hernández-Ávila, J. L. Measurement of electron drift, diffusion, and effective ionization coefficients in the SF_6 - CHF_3 and SF_6 - CF_4 gas mixtures. *J. Phys. D: Appl. Phys.* **2003**, *36*, 3132–3137.
- (17) Chervy, B.; Riad, H.; Gleizes, A. Calculation of the interruption capability of SF_6 - CF_4 and SF_6 - C_2F_6 mixtures. I. Plasma properties. *IEEE Trans. Plasma Sci.* **1996**, *24*, 198–209.
- (18) Chervy, B.; Gonzalez, J.-J.; Gleizes, A. Calculation of the interruption capability of SF_6 - CF_4 and SF_6 - C_2F_6 mixtures-Part II: Arc decay modeling. *IEEE Trans. Plasma Sci.* **1996**, *24*, 210–217.
- (19) Ahn, N.-G.; Kang, S.-W.; Min, B.-H.; Suh, S.-S. Adsorption Isotherms of Tetrafluoromethane and Hexafluoroethane on Various Adsorbents. *J. Chem. Eng. Data* **2006**, *51*, 451–456.
- (20) Müller, E. A. Adsorption of Super Greenhouse Gases on Microporous Carbons. *Environ. Sci. Technol.* **2005**, *39*, 8736–8741.

- (21) Kowalczyk, P.; Holyst, R. Efficient Adsorption of Super Greenhouse Gas (Tetrafluoromethane) in Carbon Nanotubes. *Environ. Sci. Technol.* **2008**, *42*, 2931–2936.
- (22) Jagiello, J.; Bandosz, T. J.; Putyera, K.; Schwarz, J. A. Adsorption near Ambient Temperatures of Methane, Carbon Tetrafluoride, and Sulfur Hexafluoride on Commercial Activated Carbons. *J. Chem. Eng. Data* **1995**, *40*, 1288–1292.
- (23) Choi, S. W.; Hong, S.-M.; Park, J.-H.; Beum, H. T.; Lee, K. B. CF₄ Adsorption on Microporous Carbons Prepared by Carbonization of Poly(vinylidene fluoride). *Ind. Eng. Chem. Res.* **2015**, *54*, 8561–8568.
- (24) Heuchel, M.; Snurr, R. Q.; Buss, E. Adsorption of CH₄–CF₄ Mixtures in Silicalite: Simulation, Experiment, and Theory. *Langmuir* **1997**, *13*, 6795–6804.
- (25) Yuan, X.; Choi, S. W.; Jang, E.; Lee, K. B. Chemically activated microporous carbons derived from petroleum coke: Performance evaluation for CF₄ adsorption. *Chem. Eng. J.* **2018**, *336*, 297–305.
- (26) Choi, S. W.; Lee, D.-H.; Kim, J.; Kim, J.; Park, J.-H.; Beum, H. T.; Lim, D.-S.; Lee, K. B. A titanium carbide-derived novel tetrafluoromethane adsorbent with outstanding adsorption performance. *Chem. Eng. J.* **2017**, *311*, 227–235.
- (27) Cho, D.-W.; Kim, W. S.; Chang, H.; Jung, T. S.; Park, J.; Park, J.-H. Adsorption and desorption dynamics of CF₄ on activated carbon beds: Validity of the linear driving force approximation for pressure-changing steps. *Korean J. Chem. Eng.* **2017**, *34*, 2922–2932.
- (28) Peng, X.; Vicent-Luna, J. M.; Jin, Q. Separation of CF₄/N₂, C₂F₆/N₂, and SF₆/N₂ Mixtures in Amorphous Activated Carbons Using Molecular Simulations. *ACS Appl. Mater. Interfaces* **2020**, *12*, 20044–20055.
- (29) Jagiello, J.; Bandosz, T. J.; Putyera, K.; Schwarz, J. A. Micropore Structure of Template-derived Carbons studied using Adsorption of Gases with Different Molecular Diameters. *J. Chem. Soc., Faraday Trans.* **1995**, *91*, 2929–2933.
- (30) Furmaniak, S.; Terzyk, A. P.; Gauden, P. A.; Kowalczyk, P.; Harris, P. J. F.; Koter, S. Applicability of molecular simulations for modelling the adsorption of the greenhouse gas CF₄ on carbons. *J. Phys.: Condens. Matter* **2013**, *25*, 015004.
- (31) Singh, S.; Tezel, F. H.; Harlick, P. J. E. Adsorption of Tetrafluoromethane and Nitrogen by Various Adsorbents. *Sep. Sci. Technol.* **2002**, *37*, 2763–2784.
- (32) Senkowska, I.; Barea, E.; Navarro, J. A. R.; Kaskel, S. Adsorptive capturing and storing greenhouse gases such as sulfur hexafluoride and carbon tetrafluoride using metal-organic frameworks. *Microporous Mesoporous Mater.* **2012**, *156*, 115–120.
- (33) Branken, D. J.; Krieg, H. M.; Lachmann, G.; Carstens, P. A. B. Modelling sorption and diffusion of NF₃ and CF₄ in Teflon AF perfluoropolymer membranes. *J. Membr. Sci.* **2014**, *470*, 294–306.
- (34) Skarmoutsos, I.; Koukaras, E. N.; Galiotis, C.; Froudakis, G. E.; Klontzas, E. Porous carbon nanotube networks and pillared graphene materials exhibiting high SF₆ adsorption uptake and separation selectivity of SF₆/N₂ fluid mixtures: A comparative molecular simulation study. *Microporous Mesoporous Mater.* **2020**, *307*, 110464.
- (35) Skarmoutsos, I.; Eddaoudi, M.; Maurin, G. Highly tunable sulfur hexafluoride separation by interpenetration control in metal organic frameworks. *Microporous Mesoporous Mater.* **2019**, *281*, 44–49.
- (36) Skarmoutsos, I.; Tamiolakis, G.; Froudakis, G. E. Highly selective separation and adsorption-induced phase transition of SF₆-N₂ fluid mixtures in three-dimensional carbon nanotube networks. *J. Supercrit. Fluids* **2016**, *113*, 89–95.
- (37) Tylianakis, E.; Dimitrakakis, G. K.; Melchor, S.; Dobado, J. A.; Froudakis, G. E. Porous Nanotube Network: a Novel 3-D Nanostructured Material with Enhanced Hydrogen Storage Capacity. *Chem. Commun.* **2011**, *47*, 2303–2305.
- (38) Dimitrakakis, G. K.; Tylianakis, E.; Froudakis, G. E. Pillared Graphene: A New 3-D Network Nanostructure for Enhanced Hydrogen Storage. *Nano Lett.* **2008**, *8*, 3166–3170.
- (39) Nugent, P.; Belmabkhout, Y.; Burd, S. D.; Cairns, A. J.; Luebke, R.; Forrest, K.; Pham, T.; Ma, S.; Space, B.; Wojtas, L.; Eddaoudi, M.; Zaworotko, M. J. Porous materials with optimal adsorption thermodynamics and kinetics for CO₂ separation. *Nature* **2013**, *495*, 80–84.
- (40) Dellis, D.; Samios, J. Molecular force field investigation for Sulfur Hexafluoride: A computer simulation study. *Fluid Phase Equilib.* **2010**, *291*, 81–89.
- (41) Potoff, J. J.; Siepmann, J. I. Vapor-liquid equilibria of mixtures containing alkanes, carbon dioxide, and nitrogen. *AIChE J.* **2001**, *47*, 1676–1682.
- (42) Jorgensen, W. L.; Maxwell, D. S.; Tirado-Rives, J. Development and testing of the OPLS All-Atom force field on conformational energetics and properties of organic liquids. *J. Am. Chem. Soc.* **1996**, *118*, 11225–11236.
- (43) Panagiotopoulos, A. Z. Direct determination of phase coexistence properties of fluids by Monte Carlo simulation in a new ensemble. *Mol. Phys.* **1987**, *61*, 813–826.
- (44) Dubbeldam, D.; Calero, S.; Ellis, D. E.; Snurr, R. Q. RASPA: molecular simulation software for adsorption and diffusion in flexible nanoporous materials. *Mol. Simul.* **2016**, *42*, 81–101.
- (45) Peng, D.-Y.; Robinson, D. B. A New Two-Constant Equation of State. *Ind. Eng. Chem. Fundam.* **1976**, *15*, 59–64.
- (46) Allen, M. P.; Tildesley, D. J. *Computer Simulations of Liquids*; Oxford University Press: Oxford, 1987.
- (47) Hoover, W. G. Canonical dynamics: Equilibrium phase-space distributions. *Phys. Rev. A: At., Mol., Opt. Phys.* **1985**, *31*, 1695–1697.
- (48) Smith, W.; Forester, T. R. DL_POLY_2.0: a general-purpose parallel molecular dynamics simulation package. *J. Mol. Graphics* **1996**, *14*, 136–141.
- (49) Skarmoutsos, I.; Kampanakis, L. I.; Samios, J. Investigation of the vapor-liquid equilibrium and supercritical phase of pure methane via computer simulations. *J. Mol. Liq.* **2005**, *117*, 33–41.
- (50) Potter, S. C.; Tildesley, D. J.; Burgess, A. N.; Rogers, S. C. A transferable potential model for the liquid-vapour equilibria of fluoromethanes. *Mol. Phys.* **1997**, *92*, 825–833.
- (51) Matito-Martos, I.; Álvarez-Ossorio, J.; Gutiérrez-Sevillano, J. J.; Dobaré, M.; Martín-Calvo, A.; Calero, S. Zeolites for the selective adsorption of sulfur hexafluoride. *Phys. Chem. Chem. Phys.* **2015**, *17*, 18121–18130.
- (52) Builes, S.; Roussel, T.; Vega, L. F. Optimization of the separation of sulfur hexafluoride and nitrogen by selective adsorption using monte carlo simulations. *AIChE J.* **2011**, *57*, 962–974.